







High-performance ultra-low- k fluorine-doped nanoporous organosilica films for inter-layer dielectric

Ganglong Li¹ , Guang Zheng¹, Zijun Ding², Lei Shi¹, Junhui Li¹, Zhuo Chen^{1,*} , Liancheng Wang¹ , Andrew A. O. Tay³, and Wenhui Zhu^{1,*} 

¹ State Key Laboratory of High Performance Complex Manufacturing, College of Mechanical and Electrical Engineering, Central South University, Changsha 410083, China

² State Key Laboratory of ASIC and System, School of Microelectronics, Fudan University, Shanghai 200433, China

³ Singapore University of Technology and Design, Singapore 487372, Singapore

Received: 10 July 2018

Accepted: 9 October 2018

Published online:
22 October 2018

© Springer Science+Business
Media, LLC, part of Springer
Nature 2018

ABSTRACT

Development of low- k materials is critical for further improving the performance of integrated circuits. In this work, a novel type of fluorine-doped ultra-low- k porous SiCOH films has been produced. The chemical composition and bond configurations of the nanometer-scale porous films were determined using Fourier transform infrared spectroscopy and X-ray photoelectron spectroscopy. A low dielectric constant of 2.15 was achieved with an elastic modulus of 4.84 GPa which is significantly larger than the minimum requirement of 4 GPa for ultra-large-scale integrated circuit inter-layer dielectric applications. The cage/net Si–O–Si ratio method has been proposed to elucidate the influence of molecular structure on the mechanical properties of the film. The breaking and remaking of certain bonds under UV irradiation results in the formation of increased amounts of the net Si–O–Si molecular configuration which plays a major role in increasing the elastic modulus of the film. Furthermore, it was found that increase in elastic modulus is proportional to the duration of irradiation and an increase of 20% can be achieved after 4 h of UV irradiation. The methodology and approach described in this paper can be further followed to study the mechanical properties of ultra-low k materials under various annealing and porosity conditions, and to use fluorine-doping and UV irradiation processes for optimum ultra-low k materials in application.

Introduction

As integrated circuits (ICs) continue to move toward high speeds, high densities, low power consumption, and multi-functions, the resistances of the inter-metal

and inter-layer dielectrics are dramatically increasing due to the shrinking of feature size [1–4]. Signal delay and cross-talk noise increases as the parasitic resistance–capacitance product (RC delay) raises. Therefore, RC delay in the multilevel interconnections has

Address correspondence to E-mail: zhuochen@csu.edu.cn; zhuwenhui@csu.edu.cn

become the determining factor in the over-all chip performance [5]. However, it is particularly difficult to reduce the RC delay simply by using low-resistance materials. Fu et al. showed that using Ag instead of Cu only reduced by 6% of the parasitic capacitance [6].

Porous SiCOH films are developed as the dielectric in the metal interconnections in ULSI, insulating the metal line network to reduce the RC delay, and therefore, the development of low- k materials is critical for further improving the performance of ICs [7]. Further reductions in dielectric constant have been reported by adopting sol-gel processes, chemical vapor deposition (CVD), and plasma-enhanced chemical vapor deposition (PECVD) for preparing fluorinated silicon dioxide films (FSG), organic film [6], carbon-based film (a-C:F, DLC, FDLC, a-CN_x, BCN) [7–10], and carbon-doped silicon-oxide film (SiCOH) [11–13]. A step beyond SiCOH, to continually support scaling-down is to introduce porosity in the film using PECVD techniques [14–16]. Researchers have also found that high-density nanopores can reduce dielectric constant. However, nanopores increase the diffusion channel of Cu atoms, leading to increase in leakage current and the reduction in breakdown voltage. As the porosity and the pore size are increased, the pore connectivity is strengthened, and this will lead to moisture absorption, contamination, and deterioration of mechanical properties. Based on this, scholars have reported on the effect of the porosity on the k value [14, 17]. But there are only a few reports on the mechanism of the effect of nanopores on the mechanical properties from the perspective of molecular structure and bonds evolution of low- k materials. As a chemical mechanical polishing (CMP) process is required to flatten the layer of low- k materials deposited on a substrate, a Young's modulus greater than 4 GPa, and hardness greater than 0.5 GPa [18], are usually required to meet the multilayer wiring requirements in back end of line (BEoL). UV irradiation treatment, plasma surface treatment, and electron beam curing are commonly used to improve the mechanical strength of the low- k materials to avoid cracking and deformation during the CMP process. Since UV irradiation treatment can be performed at room temperature without increasing the dielectric constant, it is widely used to improve the mechanical properties of thin films [19]. However, the mechanism of the effect of

UV irradiation on the mechanical properties of low- k materials is still unknown.

This paper describes the development and characterization of a novel fluorine-doped ultra-low- k porous SiCOH film (F-pSiCOH). The low-density porous dielectrics films were prepared using PECVD. The chemical composition of the film was analyzed using X-ray photoelectron spectroscopy (XPS), while the bond configurations were analyzed using Fourier transform infrared spectroscopy (FTIR). The porosity and pore sizes were measured using an ellipsometric porosimeter (EP). Based on the above analyses, the effect of nanopores on the mechanical properties of the F-pSiCOH film was studied. The effect of UV irradiation treatment on the structural and mechanical properties of the F-pSiCOH films was also investigated.

Experimental procedure

Fabrication of the F-pSiCOH films

The F-pSiCOH films were grown in a parallel-plate PECVD reactor, using methyltriethoxysilane (MTES; C₇H₁₈O₃Si), porogen cinene (LIMO; C₁₀H₁₆) as precursors, C₂F₆ as fluorinating agent, and helium as carrier gas. The substrates used were 300-mm-diameter, low-resistivity silicon wafers that were pre-cleaned through the RCA cleaning process. The plasma was generated using radio frequency (RF) power supply with a frequency of 13.56 MHz between the two electrodes. The films were deposited at 200 °C with an RF power of 500 W and a working pressure of 3 torr. The flow rate of the C₂F₆ was maintained at 500 sccm, as shown in Fig. 1a, b, and the F-pSiCOH films with thickness varying from 980 nm to 1124 nm were prepared after 9 min deposition. Subsequently, to remove the porogen fragments and obtain nanoporous films, they were annealed at 420 °C in N₂ for 4 h at atmospheric pressure. To investigate the effect of porogen cinene (LIMO) on the properties of the film, five flow rates of LIMO were used, varying from 1 g/min to 2 g/min, resulting in five samples of the film with different compositions as shown in Table 1.

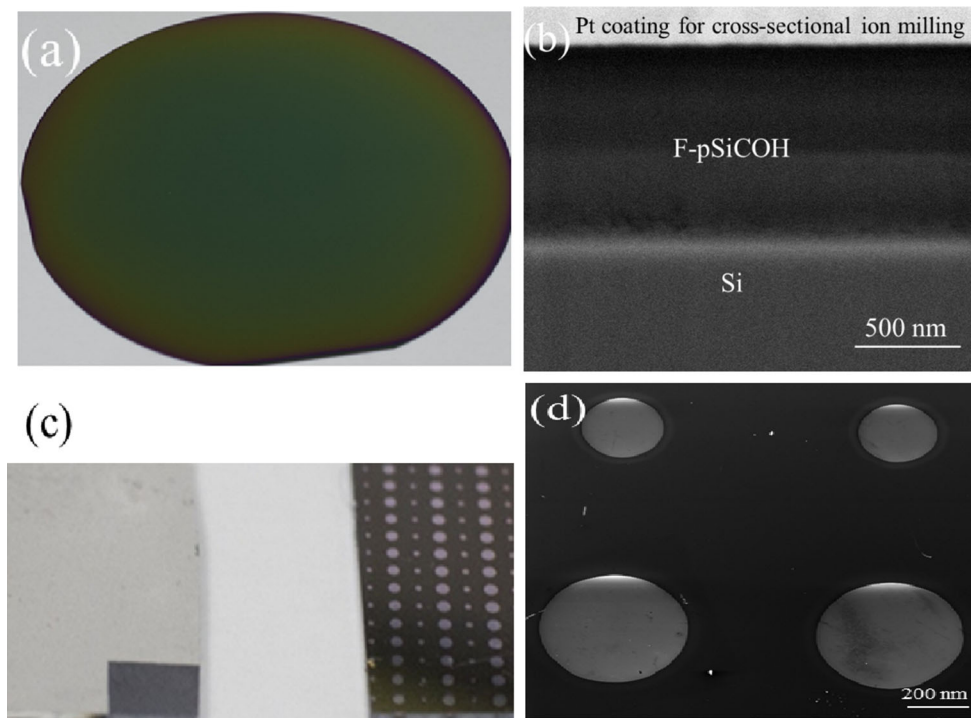


Figure 1 **a** Picture of a 4" wafer coated with the F-pSiCOH layer, **b** the cross-sectional SEM image, **c** the picture of MIS structure, and **d** SEM image of the electrode patterning for C–V measurement.

Characterization

Figure 1c shows a metal–insulator–semiconductor (MIS) structure that was used to measure the dielectric constant characteristics of F-pSiCOH films. As shown in Fig. 1d the circular patterns of high purity Al metal (99.99%) of diameter 650 μm and thickness 200 nm were sputtered onto the substrate using a shadow mask. To form ohmic contacts, Al metal of 100 nm was sputtered onto the whole back surface of the p-Si (100) wafer substrate. The dielectric constant was calculated using the capacitance–voltage (C–V) which was obtained using a precision impedance analyzer (4294A, Agilent Technologies, Malaysia) at room temperature, relative humidity of 60%, and standard atmospheric pressure.

Fourier transform infrared spectroscopy and X-ray photoelectron spectroscopy were employed to characterize the chemical bonds and compositions of the

films. The surface morphologies of the films were observed using atomic force microscopy (AFM). An ellipsometric porosimeter was used to determine the porosity, pore size, and thickness of the films (GAM-100, Leuven Instrument, China). The hardness and elastic modulus of the films were determined using nanoindentation (G200, Agilent, Inc., USA).

Results and discussion

Characterization of F-pSiCOH film

Chemical bonds of the as-deposited films

Figure 2 shows the FTIR spectra of the as-deposited films with different LIMO mass flow rates. An absorption peak with wave number at around 930 cm^{-1} indicates the existence of a Si–F bond [20],

Table 1 Mass flow rate of components used in fabricating F-pSiCOH films using PECVD

| | Sample A | Sample B | Sample C | Sample D | Sample E |
|--------------------------------------|----------|----------|----------|----------|----------|
| LIMO (g/min) | 1 | 1.2 | 1.5 | 1.7 | 2 |
| METS (g/min) | 1 | 1 | 1 | 1 | 1 |
| C ₂ F ₆ (sccm) | 500 | 500 | 500 | 500 | 500 |

confirming that low-polarity F has been successfully incorporated into the films. The strongest absorption band between 950 and 1250 cm^{-1} is associated with the Si–O–Si (around 1050 cm^{-1}) configuration [21], which serves as the backbone of the molecular structure of the F-pSiCOH film. Absorption peaks at around 1080 cm^{-1} represent the C–F bonds stretching mode in $=\text{CF}_2$ and $\equiv\text{CF}$ [20]. Furthermore, the absorption peak at 1270 cm^{-1} originates from the symmetrical deformation vibration of $-\text{CH}_3$ in $\text{Si}-\text{CH}_3$, and the peaks between 780 cm^{-1} and 850 cm^{-1} correspond to the C–H rocking vibration in $\text{Si}-\text{CH}_3$ [21, 22]. The absorption peak observed between 2800 – 3000 cm^{-1} corresponds to the CH_x group [21, 23].

As the flow rate of porogen LIMO is increased, the absorption peaks corresponding to $\text{Si}-\text{CH}_3$ ($\sim 1270\text{ cm}^{-1}$, 780 – 850 cm^{-1}), $-\text{CH}_x$ (2800 – 3000 cm^{-1}) and Si–F bonds (930 cm^{-1}) exhibit similar patterns. However, the absorption band between 950 and 1250 cm^{-1} shows an obvious change. Since there are many groups in the region of 950 – 1250 cm^{-1} , these groups will interact and make their peaks change (for example, redshift or blueshift).

Chemical bonds of the annealed films

To study the effect of annealing treatment on the porous microstructure of the F-pSiCOH films, the FTIR spectra of the films after annealing at $420\text{ }^\circ\text{C}$ for 4 h, were obtained and compared with that of the as-deposited film in Fig. 3. For the annealed film, the absorption peak corresponding to the CH_x groups

becomes weak. This indicates that the organic components ($-\text{CH}_x$) originating from LIMO during PECVD are effectively decomposed, thus producing nanopores in the film. Moreover, note that the peak associated with the Si– CH_3 (near 1270 cm^{-1}) is retained after annealing. This reflects that the Si– CH_3 groups within the molecular structure have good thermal stability, thus ensuring the retention of low- k properties after high-temperature annealing. Furthermore, the FTIR spectra of the as-deposited film do not show any peaks from OH groups or H_2O molecules, while after annealing, the absorption peak corresponding to the OH group appears in the range of 3500 – 4000 cm^{-1} . This suggests that the nanopores can lead to hydrophilicity after annealing.

In order to quantify the content of the various molecular configurations in the F-pSiCOH film fabricated, FTIR spectra for wave numbers in the range from 1000 to 1250 cm^{-1} for different samples were deconvoluted by using the origin 8.5 software as shown in Fig. 4. The peak at 1037 cm^{-1} in Fig. 4 is attributed to an open-linked silicon suboxide (Fig. 5a), since the silicon atoms prefer to neighbor one or more non-oxygen atoms. The atomic electronegativity theory [24] indicates that an atom attracts the bonding electrons in the Si–X (non-oxygen) bond less strongly than oxygen in the Si–O bond, thus distorting the tetrahedra and reducing the bond angle to $<144^\circ$. The peak centered around 1095 cm^{-1} corresponds to the net Si–O–Si configuration, and the bond angle is approximately 144° (Fig. 5b). The peak at 1157 cm^{-1} corresponds to the cage Si–O–Si configuration (Fig. 5c) [25–27]. The

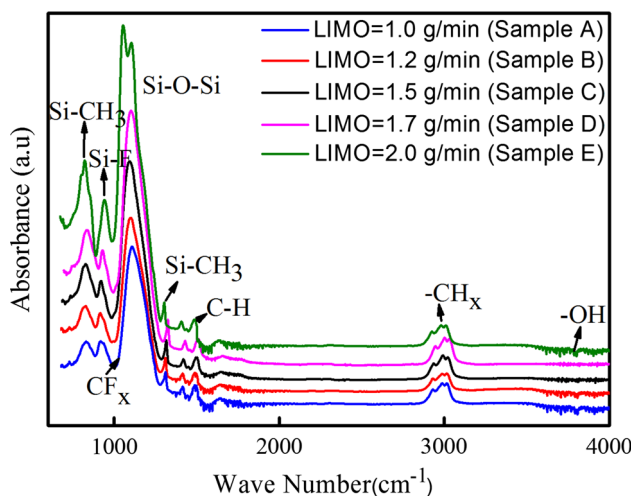


Figure 2 FTIR spectra of the as-deposited film samples.

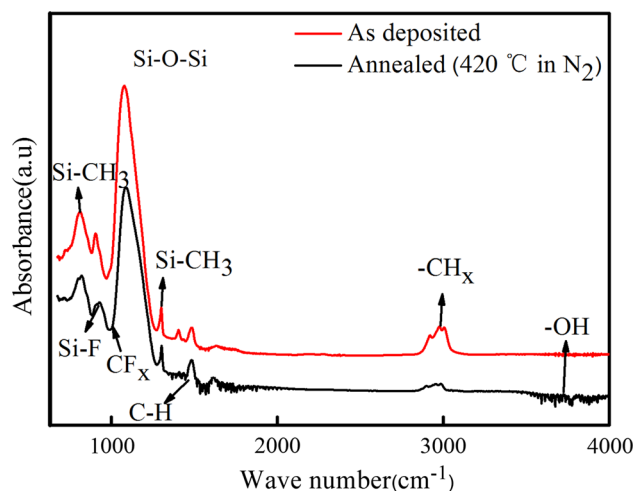


Figure 3 FTIR spectra of Sample C: As-deposited and Annealed.

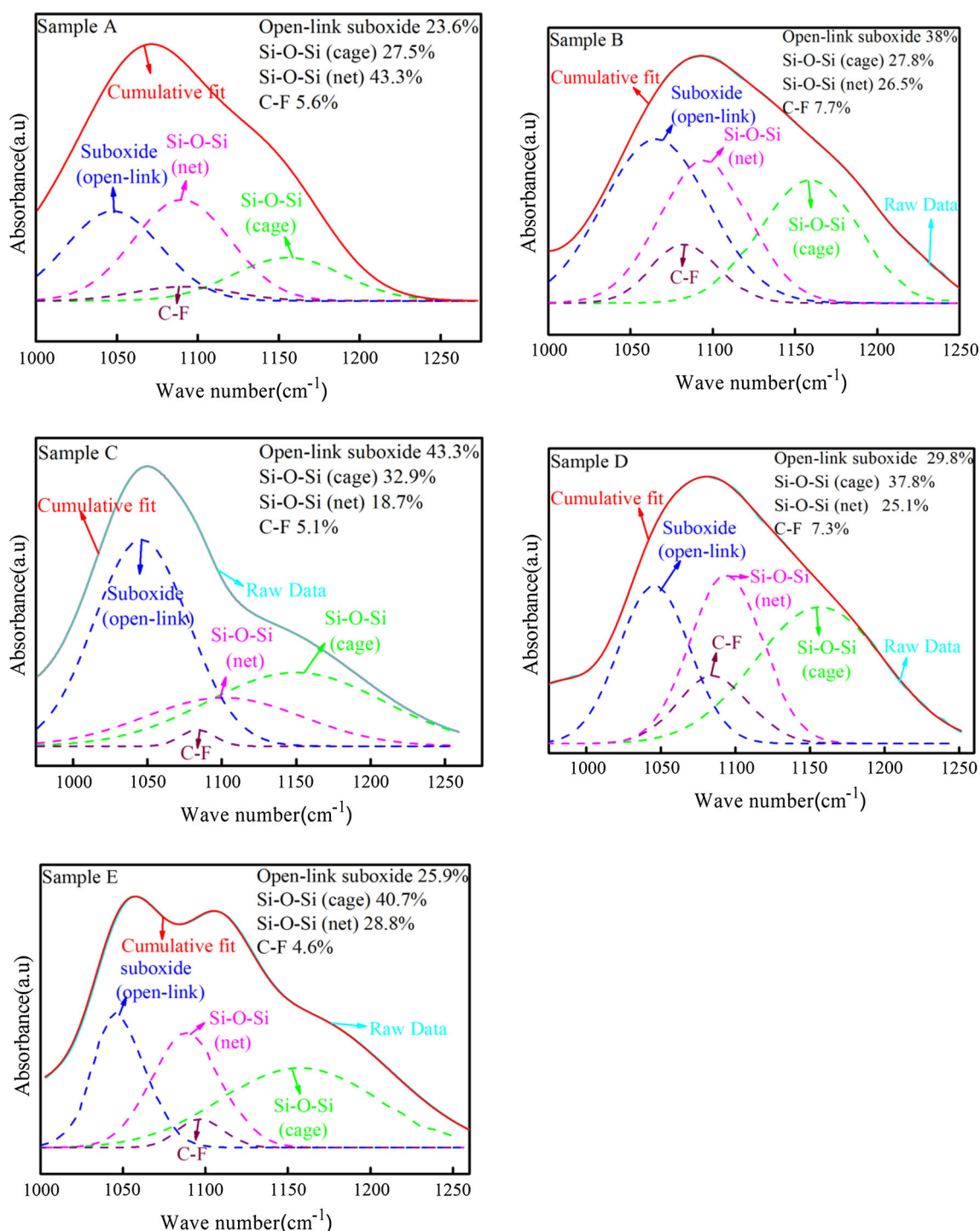


Figure 4 Gaussian functions of FTIR spectra in the range of 1000–1250 cm^{-1} for F-pSiCOH.

absorption peak areas were obtained by Gaussian integration of the deconvoluted distributions, and the percentage of the area is proportional to the relative content of the molecular configurations in F-pSiCOH.

As can be seen from the comparison of five samples in Fig. 4, when LIMO flow rate is increased, the

content of open-linked Si suboxide first increases, reaches a maximum at LIMO flow rate of 1.5 g/min, and then decreases. The cage Si–O–Si configuration increases continually with LIMO flow rate. On the other hand, the net Si–O–Si configuration first decreases, reach a minimum at a LIMO flow rate of

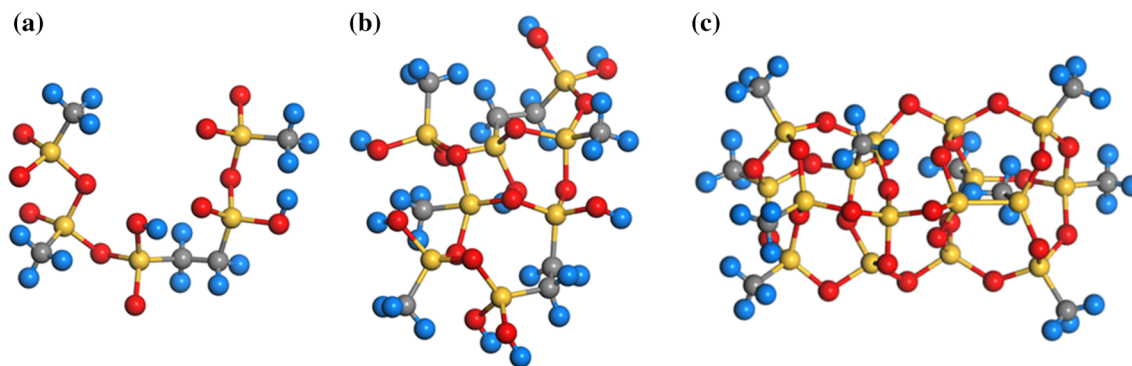


Figure 5 Schematic diagrams of the backbone structures of the Si–O groups: **a** open-linked silicon suboxide, **b** net Si–O–Si structures, **c** Cage Si–O–Si structures. Yellow-colored atoms are Si, gray are C, red are O and blue are H.

1.5 g/min and then increases. The C–F configuration appears to remain roughly constant in content between 4.6% and 7.7%.

Chemical composition of the F-pSiCOH films

The chemical composition of the prepared F-pSiCOH films was determined using XPS. All XPS data were collected using a VG Theta 300 XPS system equipped with a hemispherical analyzer and an Al anode X-ray source (1486.6 eV). The emitted photoelectrons were detected using a pass energy level of 20 eV for high-resolution scans of the Si 2p, C 1s, F 1s and O 1s core levels [28]. XPS depth profiling was performed using a 5-k eV Ar⁺ ion sputtering beam. The surface of the film was bombarded with an Al target for 10 min, and the sample was calibrated with carbon. Figure 6 shows the high-resolution XPS spectra for Sample A, C and E. The films are composed of Si, O, and C, which originate from MTES and LIMO, and F was incorporated into the films from C₂F₆. The chemical composition of the sample C was determined to be 3.46% F, 16.15% C, 27.66% Si, and 52.73% O.

As shown in Fig. 7a the XPS spectrum for Si2p can be deconvoluted into three Gaussian peaks, which correspond to Si–F (104.8 eV), C–Si–O₃ (102.5 eV) and Si–O (103.6 eV) [29, 30], respectively. The relative area percentage of each component indicates that the easiest to form are Si–O bonds, which are usually contained in net Si–O–Si and cage Si–O–Si and open-link silicon suboxide configurations which cannot be cross-linked. The relative content of Si–F is small, but since the polarity of Si–F is smaller than that of Si–O, it can effectively reduce the dielectric constant. Figure 7b shows the O1s XPS spectra for the prepared films, which can be well deconvoluted into two

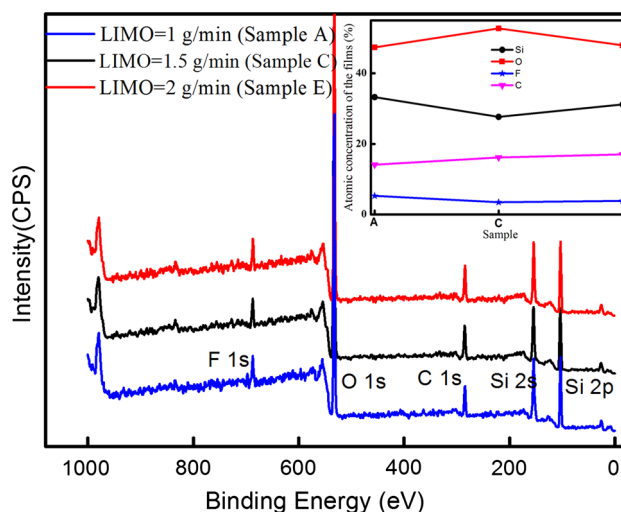


Figure 6 XPS spectra of all components in Sample A, C and E.

Gaussian peaks assigned to Si–O–Si (532.8 eV) and Si–OH (533.4 eV) bonds, respectively. The bonds of Si–OH demonstrate once again the existence of –OH in the range of 3000–4000 cm^{−1} in Fig. 2. Meanwhile, Fig. 7c shows the high-resolution C1s XPS spectra of Sample C in which three Gaussian peaks corresponding to Si–CH (283.8 eV), C–C/C–H (284.8 eV), and C–CF (287 eV) bonds can be observed [29, 31, 32].

Porosity of F-pSiCOH films

The porosity of annealed F-pSiCOH films, Sample A to Sample E, fabricated with mass flow rate of porogen LIMO increasing from 1 g/min to 2 g/min (Table 1) was measured using an ellipsometric porosimeter. Using N₂ as a carrier gas (*P*₀ is the N₂ pressure), the adsorbent, IPA, (*P* is the pressure), was brought to the surface of the sample. Due to the capillary force, the adsorbent was adsorbed into the

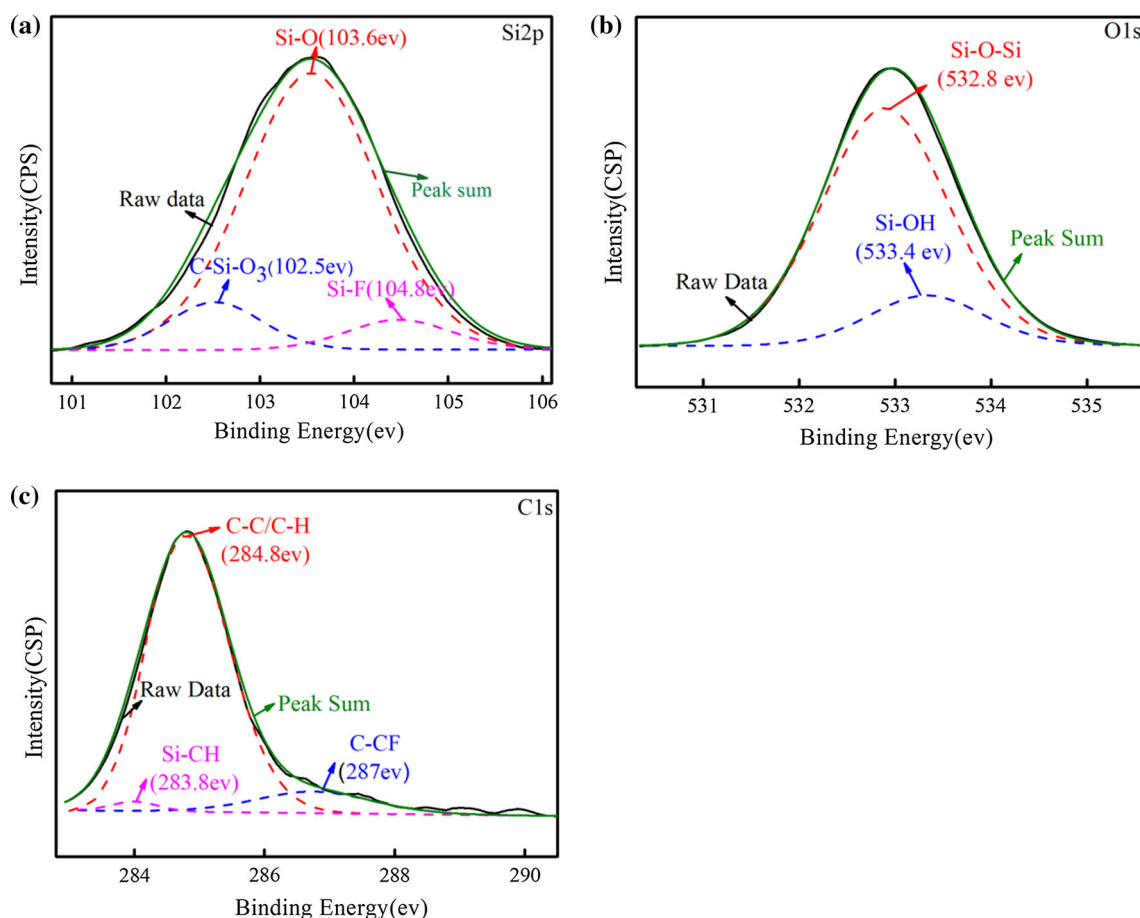


Figure 7 High-resolution XPS spectra of Sample C: **a** Si2p; **b** O1s; and **c** C1s.

sample pores and the adsorbent content was gradually increased until the relative pressure (P_0/P) was 1, to yield an adsorption curve. Then the amount of adsorbent was gradually decreased. The desorption measurement was performed until the relative pressure was 0, and a desorption curve was obtained. The absorption and desorption curves for Sample C are shown in Fig. 8a. It can be seen that there is a hysteresis between the absorption and desorption curves, which demonstrates that the pores were not standard cylindrical geometry. Since we are only interested in porosity, only the desorption curves are plotted in Fig. 8b.

As can be seen in Fig. 8b, when the porogen LIMO flow rate is increased, the porosity first increases and then reaches a maximum value of 32.4% at LIMO flow rate of 1.5 g/min before decreasing. This trend can be explained by the fact that when the flow rate of porogen LIMO is increased, the incorporated porogen fragments and hence the porosity and pore size increase. However, the pore walls of the

F-pSiCOH film become thinner. On further increase in LIMO flow rate, the pores become so large that they collapse after annealing, effectively resulting in reduced porosity. This explanation is corroborated by Fig. 8c which shows the distribution of pore radius for the five different LIMO flow rates. When the mass flow rate of LIMO increases, the pore radius is increased from 0.71 nm up to a maximum of 1.1 nm (LIMO flow rate = 1.5 g/min). However, when the flow rate of LIMO is greater than 1.5 g/min, the pore radius is decreased to 0.92 nm at a LIMO flow rate of 2 g/min.

Dielectric constant and refractive index of F-pSiCOH films

From the above discussion, we can infer that the preparation conditions influence more heavily on the nanoscale pore-related structure than on the chemical composition of the film, and the different forms of Si-O structure mentioned earlier is of particular interest.

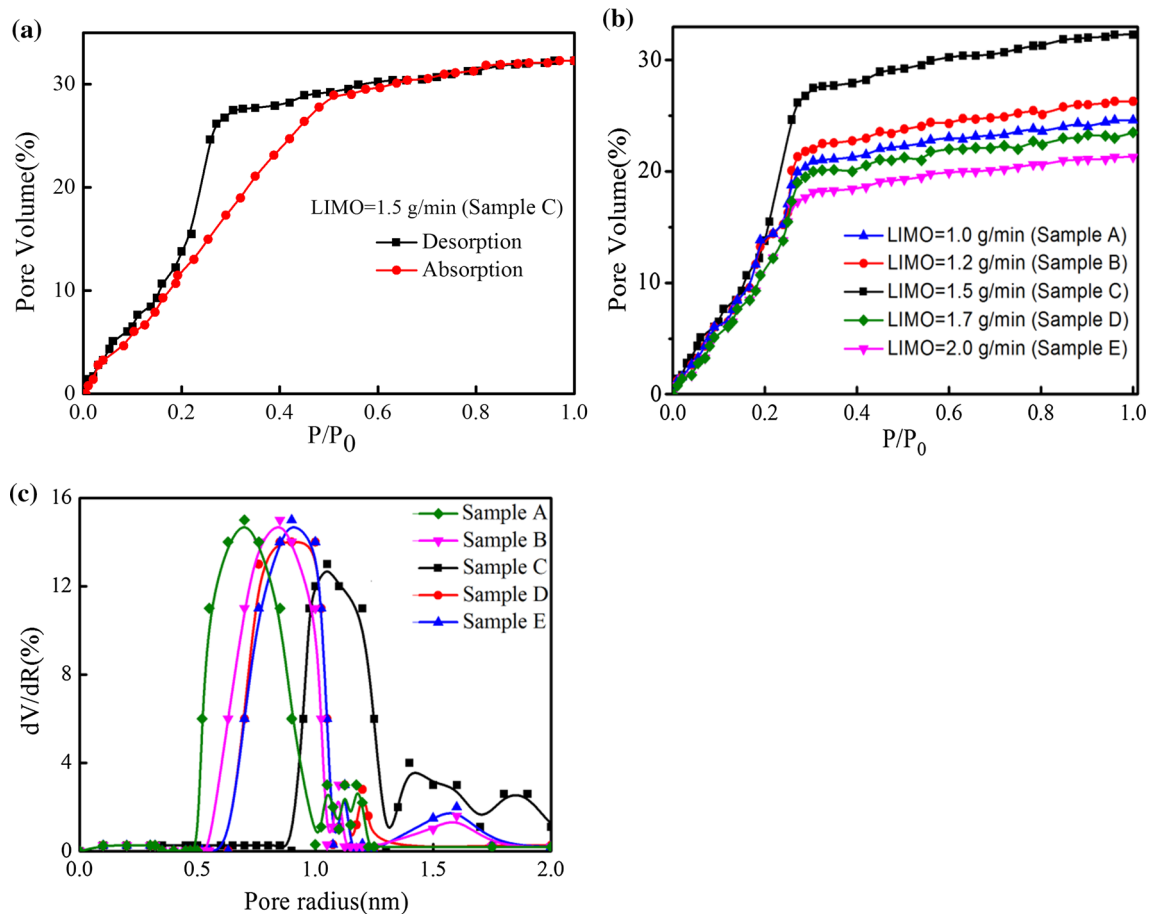


Figure 8 Variation of porosity and pore radius with LIMO flow rate. **a** IPA-sorption isotherms, **b** the pore volume of different samples, **c** pore radius distributions.

Figure 9 shows the relationship of the dielectric constant and the refractive index with the relative contents of cage Si–O–Si. As the relative content of cage Si–O–Si increases from 27.5 (Sample A) to 32.9 (Sample C), the k value decreases from 2.38 to 2.15, due to the increase in porosity of the annealed film. As the relative content of cage Si–O–Si is increased from 32.9 to 40.7 (Sample E), the k value increases to 2.45. This can be attributed to the decreased porosity within the film for LIMO flow rates greater than 1.5 g/min (section “Porosity of F-pSiCOH films”). Undoubtedly, the refractive index of the film shows a similar variation with relative contents of cage Si–O–Si. As can be seen in Fig. 4c–e, the content of cage Si–O–Si and silicon suboxide combined is reduced, and therefore, the volume of the molecular structure is also reduced, thus reducing the refractive index [25].

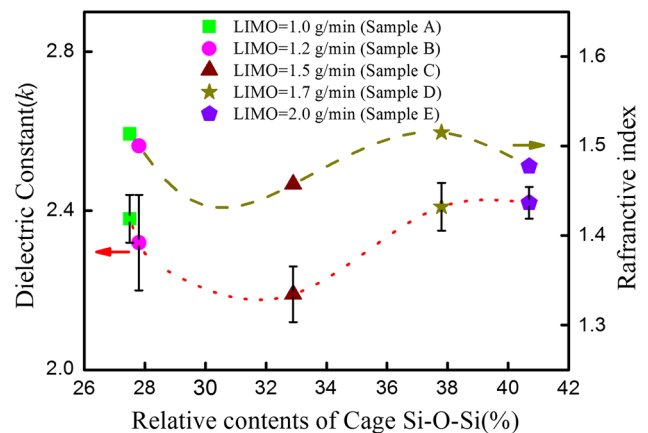


Figure 9 Variation of dielectric constant and refractive index with relative content of cage Si–O–Si.

Mechanical properties of F-pSiCOH films

Formation of the cage configuration is consistent with increasing porosity of the F-pSiCOH film, and the net Si–O–Si structure configuration also plays a key role in the mechanical property [15]. If possible, it would be desirable to correlate the mechanical properties of the film with its pore microstructure. Nanoindentation method which is proven effective in measuring elastic modulus of thin films was used here [33]. Figure 10 shows the variations of the elastic modulus (E) and the hardness (H) of the F-pSiCOH film with the ratio of cage/net Si–O–Si in the films. As can be seen, the Young's modulus decreases linearly with the ratio of cage/net Si–O–Si in the films. This can be explained by the fact that the cage Si–O–Si configuration has a large molecular free volume and hence is more compliant than the net Si–O–Si configuration. Hence, when the cage/net Si–O–Si ratio is increased, the elastic modulus of the film is decreased. From Fig. 10, it can be seen that the hardness, H , also decreases linearly when the ratio of cage/net Si–O–Si increases from 0.63 to 1.41, but beyond 1.41, H begins to show a small increase.

Effect of UV irradiation on the mechanical properties of F-pSiCOH films

We further studied the effect of UV radiation on the mechanical properties of annealed F-pSiCOH film. Wide band UV lamps with wavelengths between 200 nm and about 400 nm were used as the UV irradiation source. Various researches [34] showed that the mechanical properties of dielectric materials

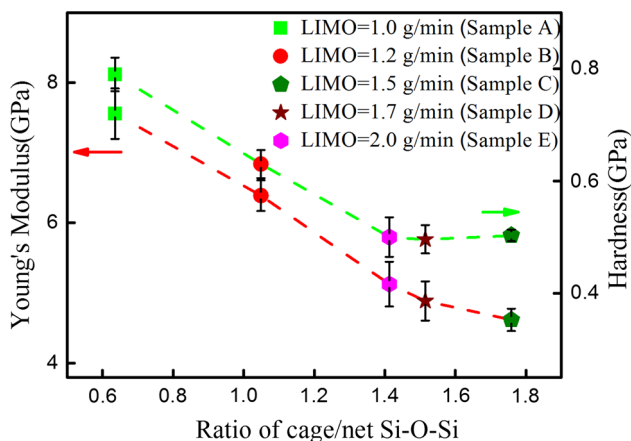


Figure 10 Variation of Young's modulus and hardness with ratio of cage/net Si–O–Si.

were improved by UV irradiation, but the k value of dielectric materials also increased after 6 h of UV irradiation. Therefore, we performed UV irradiation on the films for 4 h at most to study the mechanism of UV irradiation on the mechanical properties of the F-pSiCOH films.

FTIR spectra for UV irradiated films were obtained and compared with those for the annealed films in Fig. 11. It can be seen that after UV irradiation, the intensity of the OH (Si–OH) bond is increased, arising from exposure to the ambient atmosphere. Under UV irradiation for 4 h, it can be observed that the intensity of absorption peak 1648 cm^{-1} corresponding to the C=C/C–H groups is decreased, probably due to the cross-linking reaction of the film [35].

High-resolution XPS were used to analyze the chemical bonding structure and composition of the UV-irradiated films. The XPS spectral peaks of C1s and Si2p and O1s were fitted with the Gaussian–Lorentz function. As shown in Fig. 12, the C1s XPS spectra consists of C–C/C–H (284.8 eV), Si–CH (283.8 eV), and C–CF (287 eV) Gaussian peaks before UV irradiation. After 4 h of UV irradiation, a new peak appears at 285.9 eV, which corresponds to the C–O bond [36]. The radiation energy of UV source of such intensity can only break the weak bonds in the film, such as C–H and C–C [37]. The weak bonds generate active end groups or groups which rebounded to the same active structure around them or even became incorporated into the Si–O bond configuration. The C 1s spectra can be deconvoluted into five peaks such as Si–F (104.8 eV), C–Si–O₃ (103.6 eV), Si–O₄ (104.4 eV), O₂–Si–C₂ (102.9 eV) and O–Si–C₃ (101.9 eV). After 4 h of UV irradiation, the relative contents of the O–Si–C₃, O₂–Si–C₂, and Si–F

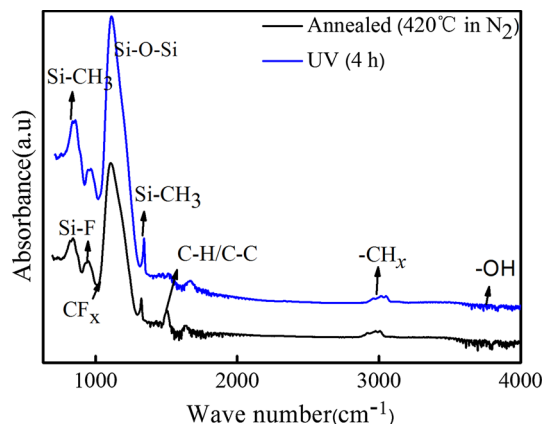


Figure 11 FTIR spectra of Sample C: Annealed, and after UV irradiation.

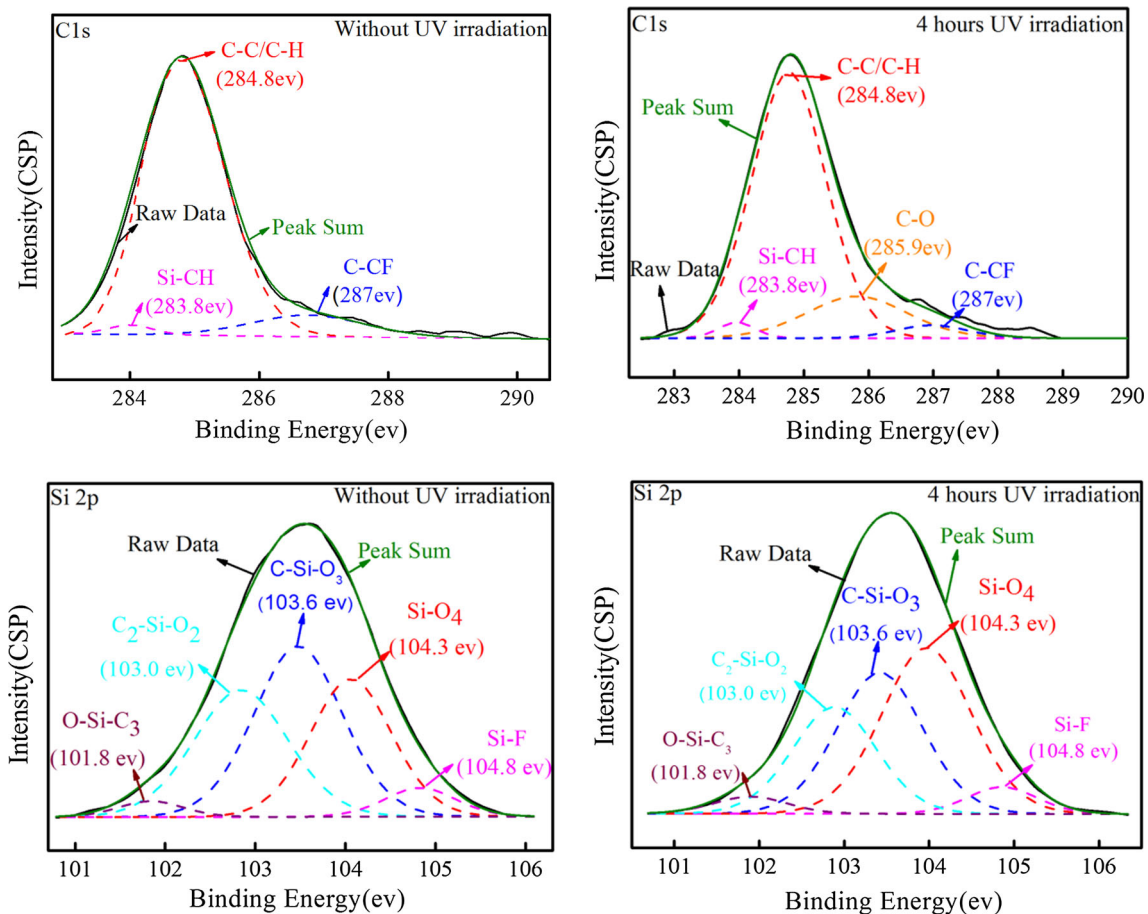


Figure 12 C1s and Si 2p XPS spectra: without UV irradiation and with 4 h of UV irradiation.

bond configurations remain unchanged, but the content of the C–Si–O₃ configuration decreases, and the content of Si–O₄ increases. The weaker chemical bond of Si–C is decomposed after UV irradiation of the film, generating a Si dangling bond which then bonds with O from air to form an Si–O bond.

Figure 13 shows the surface morphologies of the as-deposited, subsequently annealed, and UV-irradiated films. The as-deposited film has a smooth surface and the root-mean-square (RMS) roughness is 0.387 nm. For the annealed films, the RMS roughness increases to 0.554 nm. This is mainly due to the decomposition of the CH_x groups at high temperatures, resulting in a large amount of nanopores. However, for the UV-irradiated films, the RMS roughness is lower at 0.469 nm. This is because cross-linking occurs under UV irradiation, resulting in changes in the bonding configuration and a smoother surface.

Figure 14 shows the variation of elastic modulus of the F-pSiCOH film (Sample C) with duration of UV

irradiation. The elastic modulus (E) of the F-pSiCOH film without UV irradiation is 4.84 GPa. With the increase in irradiation time, the elastic modulus increases approximately linearly. This is due to the breaking of C–H/Si–C bonds under UV irradiation [36], consequent remaking of Si–O (H) or Si–C from O–Si–C [37] (Fig. 15), and eventually the increase in cross-linked networks in the Si–O–Si configuration. Since an elastic modulus larger than 4 GPa is required for the practical application of low- k thin films [18], the film developed in this work has shown favorable mechanical properties. Together with good electrical performance and good thermal stability, it can be applied to advanced Cu/low- k interconnects.

Conclusion

In this work, porous ultra-low k F-SiCOH films have been fabricated by PECVD using precursors MTES, porogen cinene LIMO, and a fluorinating agent C₂F₆,

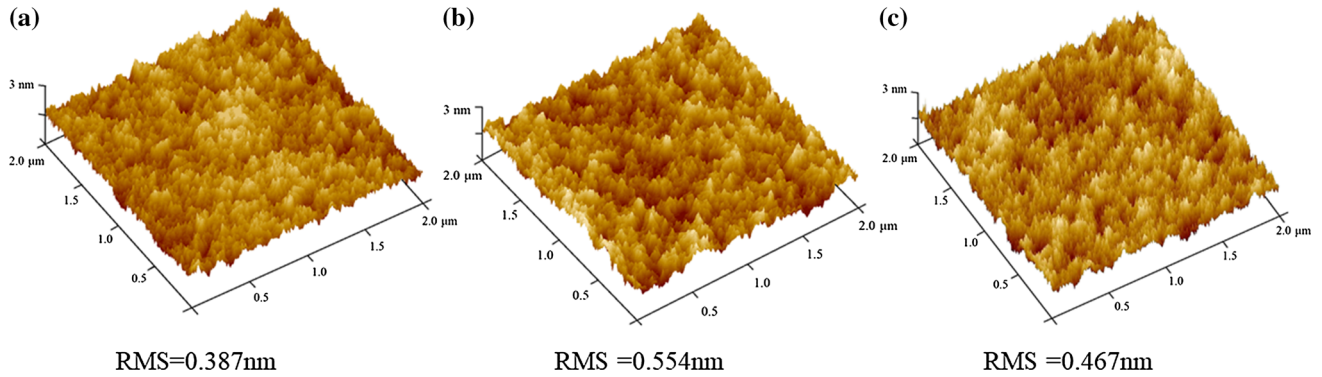


Figure 13 Surface morphologies of Sample C: **a** As-deposited, **b** annealed, **c** UV irradiated.

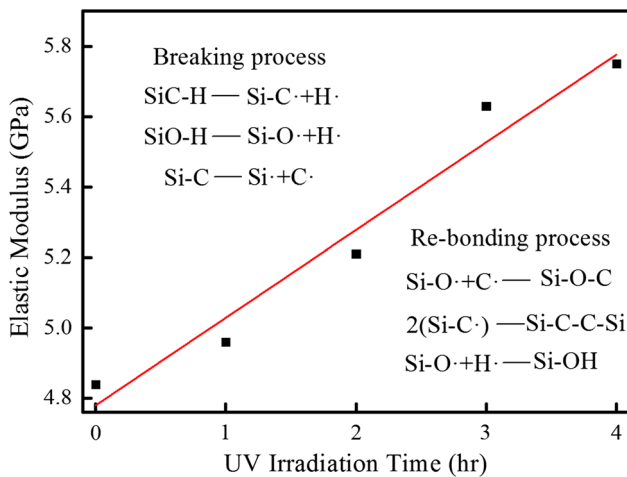
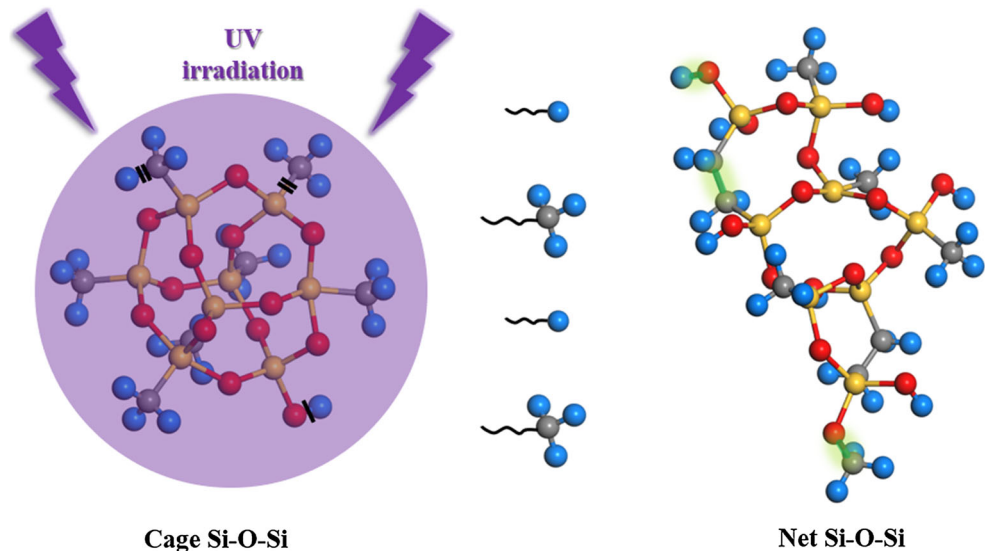


Figure 14 Variation of elastic modulus of the F-pSiCOH film with duration of UV irradiation.

Figure 15 Breaking and remaking of bonds under UV irradiation.



followed by thermal annealing and UV irradiation. A number of techniques have been used to fully characterize the properties of the film as-deposited, annealed, and after UV irradiation.

The main conclusions of this work are summarized as follows:

- (a) A fluorine-doped, ultra-low k film (F-pSiCOH) with $k = 2.15$ and $E = 4.84$ GPa has been successfully fabricated and its chemical composition, bond structure, porosity and mechanical properties characterized.
- (b) The low-polarity F has been successfully incorporated into the film to form Si-F and C-F bonds, which effectively reduced the k value.

- (c) The mass flow rate of LIMO influence the dielectric constant and mechanical properties of the film by affecting the porosity and the content of different Si–O–Si configurations. Maximum porosity of 32.4% was obtained at 1.5 g/min LIMO flow rate, and the elastic modulus of the film decreased with increasing cage/net Si–O–Si ratio.
- (d) The film developed has an elastic modulus of 4.84 GPa which is significantly greater than the minimum value of 4 GPa required for a usable ULSI inter-metal dielectric material.
- (e) The mechanism of the effect of UV irradiation on improvement in the elastic modulus of the low k film has been clarified. It is found that UV irradiation results in the emergence of dense cross-linking and formation of more net Si–O–Si configurations. The elastic modulus is found to increase linearly with the duration of UV irradiation. An increase of 20% can be achieved with 4 h of UV irradiation.

The above findings have important implications in the design of ultra-low k materials for advanced Cu/low- k interconnects.

Acknowledgements

This work was supported by National Basic Research Program of China (973 Program, No. 2015CB057206). Liancheng Wang acknowledges the Professorship Start-up Funding (No. 502045005), Innovation-Driven Project of Central South University (No. 502501003) and State Key Laboratory of High Performance Complex Manufacturing, Central South University (No. ZZYJKT2018-01).

References

- [1] Xiao C, He H, Li J, Cao S, Zhu W (2017) An effective and efficient numerical method for thermal management in 3D stacked integrated circuits. *Appl Therm Eng* 121:200–209
- [2] Borah D, Cummins C, Rasappa S et al (2018) Nanopatterning via self-assembly of a lamellar-forming polystyrene-block-poly(dimethylsiloxane) diblock copolymer on topographical substrates fabricated by nanoimprint lithography. *Nanomaterials* 8:32–43
- [3] Li H, Tie J, Li J et al (2018) High-performance sub-10-nm monolayer black phosphorene tunneling transistors. *Nano Res* 11:2658–2668
- [4] Zhang J, Zhang G, Gao Y, Sun R, Wong CP (2016) Ultra-low- κ HFPDB-based periodic mesoporous organosilica film with high mechanical strength for interlayer dielectric. *J Mater Sci* 51:7966–7976. <https://doi.org/10.1007/s10853-016-0066-6>
- [5] Maex K, Baklanov MR, Shamiryan D, Lacopi F, Brongersma SH, Yanovitskaya ZS (2006) Low dielectric constant materials for microelectronics. *J Appl Phys* 93:8793–8841
- [6] Fu S, Qian KJ, Ding SJ (2010) Characterization of ultra-low k porous organosilica thin films. In: *IEEE international conference on solid-state and integrated circuit technology*, pp 1033–1035
- [7] Aono M, Nitta S (2002) High resistivity and low dielectric constant amorphous carbon nitride films: application to low- k materials for ULSI. *Diam Relat Mater* 11:1219–1222
- [8] Grill A (2003) Diamond-like carbon coatings as biocompatible materials—an overview. *Diam Relat Mater* 12:166–170
- [9] Sakaue H, Yoshimura N, Shingubara S, Takahagi T (2003) Low dielectric constant porous diamond films formed by diamond nanoparticles. *Appl Phys Lett* 83:2226–2228
- [10] Sugiyama T, Tai T, Sugino T (2002) Effect of annealing on dielectric constant of boron carbon nitride films synthesized by plasma-assisted chemical vapor deposition. *Appl Phys Lett* 80:4214–4216
- [11] Grill A (2003) Plasma enhanced chemical vapor deposited SiCOH dielectrics: from low- k to extreme low- k interconnect materials. *J Appl Phys* 93:1785–1790
- [12] Kim HS, Xie YH, Devinentis M, Itoh T, Jenkins KA (2003) Unoxidized porous Si as an isolation material for mixed-signal integrated circuit applications. *J Appl Phys* 93:4226–4232
- [13] Yu S, Wong TKS, Hu X, Pita K (2003) The comparison of thermal and dielectric properties of silsesquioxane films cured in nitrogen and in air. *Chem Phys Lett* 380:111–116
- [14] Grill A, Patel V (2001) Ultralow- k dielectrics prepared by plasma-enhanced chemical vapor deposition. *Appl Phys Lett* 79:803–805
- [15] Grill A, Patel V, Jahnes C (1998) Novel low k dielectrics based on diamondlike carbon materials. *J Electrochem Soc* 145:1649–1653
- [16] Yang S, Mirau PA, Pai C-S, Nalamasu O, Reichmanis E, Pai JC, Obeng YS, Seputro J, Lin EK, Lee H-J, Sun J, Gidley DW (2002) Nanoporous ultralow dielectric constant organosilicates templated by triblock copolymers. *Chem Mater* 14:369–374

- [17] Lee HJ, Yang CS, Choi CK (2004) Effect of UV illumination on deposition of low-k Si-O-C(-H) films by PECVD. *Mater Sci Forum* 449–452:473–476
- [18] Dubois G, Volksen W, Magbitang T, Miller RD, Gage DM, Dauskardt RH (2010) Molecular network reinforcement of sol-gel glasses. *Adv Mater* 19:3989–3994
- [19] Yuan G-C, Xu Z, Zhang S-L (2009) Study on characteristics of a double-conductible channel organic thin-film transistor with an ultra-thin hole-blocking layer. *Chin Phys B* 18:3990–3994
- [20] Wang P-F, Ding S-J, Zhang J-Y, Zhang DW, Wang J-T, Lee WW (2001) Low-dielectric-constant α -SiCOF film for ULSI interconnection prepared by PECVD with TEOS/C4F8/O₂. *Appl Phys A* 72:721–724
- [21] Grill A, Neumayer DA (2003) Structure of low dielectric constant to extreme low dielectric constant SiCOH films: Fourier transform infrared spectroscopy characterization. *J Appl Phys* 94:6697–6707
- [22] Kim C, Jung A, Navamathavan R, Choi C, Woo JK (2008) Bonding configuration and electrical properties of carbon-incorporated low-dielectric-constant SiOC(-H) films with nano-pore structures deposited by using PECVD. *J Korean Phys Soc* 53:2621–2626
- [23] Ding ZJ, Wang YP, Liu WJ, Ding SJ, Baklanov M, Zhang DW (2018) Characterization of PECVD ultralow dielectric constant porous SiOCH films using triethoxymethylsilane precursor and cinene porogen. *J Phys D Appl Phys* 51:115103
- [24] Jensen WB (1996) Electronegativity from avogadro to pauling: part 1: origins of the electronegativity concept. *J Chem Educ* 73:11–20
- [25] Chen WC, Yen CT (2000) Effects of slurry formulations on chemical-mechanical polishing of low dielectric constant polysiloxanes: hydrido-organo siloxane and methyl silsesquioxane. *J Vac Sci Technol B Microelectron Nanometer Struct* 18:201–207
- [26] Lee LH, Chen WC, Liu WC (2002) Structural control of oligomeric methyl silsesquioxane precursors and their thin-film properties. *J Polym Sci Part A Polym Chem* 40:1560–1571
- [27] Li JG, Chu WC, Kuo SW (2015) Hybrid mesoporous silicas and microporous POSS-based frameworks incorporating evaporation-induced self-assembly. *Nanomaterials* 5:1087–1101
- [28] Zhou W, Bailey S, Sooryakumar R et al (2011) Elastic properties of porous low-k dielectric nano-films. *J Appl Phys* 110:043520. <https://doi.org/10.1063/1.3624583>
- [29] Chang YK, Kim SH, Navamathavan R, Chi KC, Jeung WY (2007) Characteristics of low- k SiOC(-H) films deposited at various substrate temperature by PECVD using DMDMS/O₂ precursor. *Thin Solid Films* 516:340–344
- [30] Verdonck P, Wang C, Le QT et al (2014) Advanced PECVD SiCOH low- k films with low dielectric constant and/or high Young's modulus. *Microelectron Eng* 120:225–229
- [31] An SJ, Navamathavan R, Lee KM, Chi KC (2008) Plasma characteristics of low- k SiOC(-H) films prepared by using plasma enhanced chemical vapor deposition from DMDMS/O₂ precursors. *Surf Coat Technol* 202:5693–5696
- [32] Ding S, Wang P, Zhang W, Wang J, Wei WL (2001) Analysis of the X-ray photoelectron spectra of a-SiOCF films prepared by plasma-enhanced chemical vapour deposition. *Chin Phys* 10:324–343
- [33] Vanstreels K, Wu C, Gonzalez M et al (2013) Effect of pore structure of nanometer scale porous films on the measured elastic modulus. *Langmuir ACS J Surf Colloids* 29:12025–12035
- [34] Jiang T, Zhu B, Ding SJ, Fan Z, Zhang D (2014) High-performance ultralow dielectric constant carbon-bridged mesoporous organosilica films for advanced interconnects. *J Mater Chem C* 2:6502–6510
- [35] Kim BR, Kang JW, Lee KY, Son JM, Ko MJ (2007) Physical properties of low- k films based on the co. *J Mater Sci* 42:4591–4602. <https://doi.org/10.1007/s10853-006-0575-9>
- [36] Yang CS, Choi CK (2006) Mechanical property of the low dielectric carbon doped silicon oxide thin film grown from MTMS/O source. *Curr Appl Phys* 6:243–247
- [37] Fu S, Qian KJ, Ding SJ (2011) Preparation and characterization of ultralow-dielectric-constant porous SiCOH thin films using 1,2-bis(triethoxysilyl)ethane, triethoxymethylsilane, and a copolymer template. *J Electron Mater* 40:2139–2148